Real-time and in situ monitoring of sputter deposition with RHEED for atomic layer controlled growth

J. P. Podkaminer, J. J. Patzner, B. A. Davidson, and C. B. Eom

---

Real-time and *in situ* monitoring of sputter deposition with RHEED for atomic layer controlled growth

J. P. Podkaminer,[1] J. J. Patzner,[1] B. A. Davidson,[1,2,3] and C. B. Eom[1,a]
[1]*Department of Materials Science and Engineering, University of Wisconsin-Madison, Madison, Wisconsin 53706, USA*
[2]*CNR-IOM/TASC National Laboratory, Trieste 34149, Italy*
[3]*Department of Physics, Temple University, Philadelphia, Pennsylvania 19122, USA*

Sputter deposition is a widely used growth technique for a large range of important material systems. Epitaxial films of carbides, nitrides, metals, oxides and more can all be formed during the sputter process which offers the ability to deposit smooth and uniform films from the research level up to an industrial scale. This tunable kinematic deposition process excels in easily adapting for a large range of environments and growth procedures. Despite the vast advantages, there is a significant lack of *in situ* analysis options during sputtering. In particular, the area of real time atomic layer control is severely deficient. Atomic layer controlled growth of epitaxial thin films and artificially layered superlattices is critical for both understanding their emergent phenomena and engineering novel material systems and devices. Reflection high-energy electron diffraction (RHEED) is one of the most common *in situ* analysis techniques during thin film deposition that is rarely used during sputtering due to the effect of the strong permanent magnets in magnetron sputter sources on the RHEED electron beam. In this work we have solved this problem and designed a novel way to deter the effect of the magnets for a wide range of growth geometries and demonstrate the ability for the first time to have layer-by-layer control during sputter deposition by *in situ* RHEED. © *2016 Author(s). All article content, except where otherwise noted, is licensed under a Creative Commons Attribution (CC BY) license (http://creativecommons.org/licenses/by/4.0/).* [http://dx.doi.org/10.1063/1.4961503]

Atomic layer controlled growth of complex thin film heterostructures is essential for the understanding and engineering of their properties. Molecular beam epitaxy (MBE) and pulsed laser deposition (PLD) techniques readily take advantage of reflection high-energy electron diffraction (RHEED) as an *in situ* diagnostic tool for determining the structure of the surface during deposition, enabling layer-by-layer control at the unit cell and sub unit cell level.[1–5] However, this powerful *in situ* analysis technique is not commonly available in conjunction with sputter deposition despite the commonality of this technique. The strong permanent magnets present in the magnetron sputter sources have deterred the inclusion of RHEED as an *in situ* analysis technique during sputter grown epitaxial thin films. This has left much unknown about the growth mechanisms (e.g., Stranski-Krastanov, Frank-van der Merwe or Volmer-Weber modes,[6,7] and layer-by-layer versus step flow) for many thin film systems deposited by the sputter technique. In order to achieve real time layer-by-layer controlled growth during sputtering this issue needs to be solved.

The observation of intensity oscillations of the RHEED specular reflection in MBE growth of semiconductors has been exploited for many years to control stoichiometry and growth rate.[1–3] The RHEED technique was then readily adapted to oxide MBE growth[4] and subsequently, high-pressure RHEED was developed for PLD by Rijnders *et al.*[5] and has been widely adopted for growing

---

[a]Author to whom correspondence should be addressed. Electronic mail: eom@engr.wisc.edu
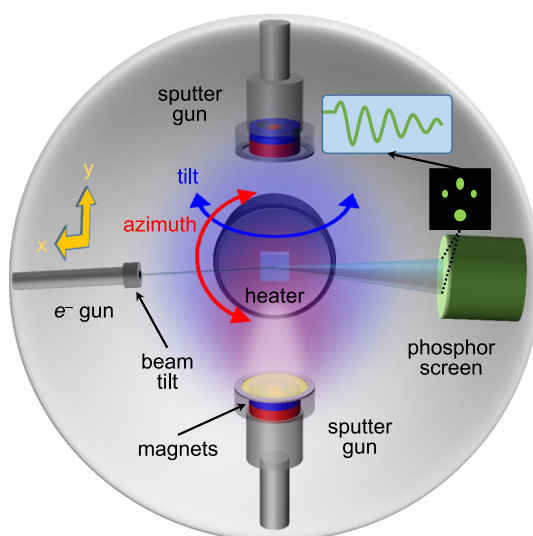
FIG. 1. Schematic of the growth chamber demonstrating the relative orientation between the heater and the sputter gun is shown along with the RHEED setup. Required degrees of freedom of the heater and electron gun are shown as the tilt and azimuth and the x, y, and beam tilt, respectively. (Multimedia view) [URL: http://dx.doi.org/10.1063/1.4961503.1]

epitaxial oxide films and controlling complex interfaces by this technique. The development of *in situ* RHEED analysis for sputter growth would introduce similar advantages-for example, rapid optimization of growth parameters and control of growth rates, and enhance reproducibility of interface and superlattice growth-to this widely used and technologically important deposition technique.[8–12]

Through finite element modeling of different experimental setups we have been able to construct a general solution for implementing RHEED with magnetron sputtering by mitigating and creating a predictable uniaxial bending of the electron beam. Using this general guideline, the major detrimental effects from the magnets can be avoided in many common sputter geometries.

In this work we choose one of the common sputter geometries that we have modeled and demonstrate digital control of magnetron sputter deposition using *in situ* high-pressure RHEED by applying this technique to the widely studied model oxide system, $SrRuO_3$ (SRO). During 90° off-axis sputtering of SRO films we observed strong specular spot oscillations that extended to more than 20 unit cells. This allows us to identify the growth mode as layer-by-layer during sputter grown SRO which is in contrast to the commonly assumed growth mode of step flow. This establishes our ability to have unit cell control during sputter growth in real time. Similar results are observed during the growth of perovskites $La_{0.7}Sr_{0.3}MnO_3$ (LSMO) and $LaAlO_3$ (LAO), confirming that this approach can be universally applied to sputter deposition of other materials.

A schematic diagram of the sputter deposition chamber setup used for this work is shown in Fig. 1. Two facing 90° off-axis sputter sources can be seen with their internal annular and button magnets. The sputter sources are shown in their relative positions with respect to the heater face and RHEED setup. Additionally, Fig. 1 indicates the relevant degrees of freedom in the system; the tilt and azimuth motions of the heater as well as the $x - y$ translation of the electron gun. The system also includes a set of bending magnets at the tip of the electron gun's differential-pumping tube denoted as "beam tilt" in Fig. 1.

Sputtering offers several challenges that have deterred the inclusion of a RHEED apparatus during growth, including strong magnetic fields around the sputter sources and high background gas pressure.[13] Consequently, the use of *in situ* RHEED with sputtering has rarely been demonstrated despite the prominent position of this deposition technique. In the RHEED geometry, an electron beam of 10-35 kV energies is directed toward the sample at grazing incidence and the diffracted beam is recorded on a phosphor screen, as demonstrated in Fig. 1. Magnetic fields produced by sputter sources will deflect the electron beam from its initial trajectory, making it difficult to observe
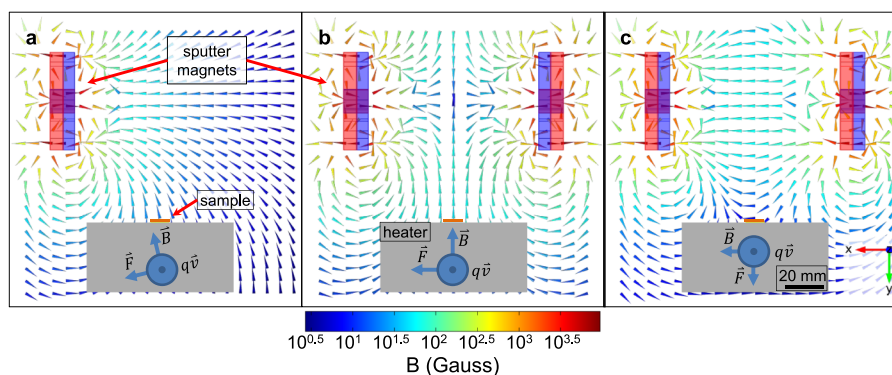
FIG. 2. 2-dimensional cross-sections showing the magnetic field close to the sample for the single gun, two gun symmetric, and two gun antisymmetric magnet polarities. The electron beam direction is into the page, and the RHEED phosphor screen is behind this plane (into the page). (a) Single gun off-axis geometry shows the magnetic field lines close to the sample are pointing nearly vertically resulting in a predominantly lateral Lorentz force. (b) Two gun symmetric off-axis geometry with the field lines close to the sample completely vertical. (c) Two gun antisymmetric geometry displays the magnetic field lines close to the sample are horizontal resulting in a Lorentz force in the y-direction. The magnitude of the magnetic field can also be compared between the three setups. (Multimedia view) [URL: http://dx.doi.org/10.1063/1.4961503.2]

the diffraction pattern. As expected, this deflection is very sensitive to the magnets' proximity and orientation with respect to the electron beam, so small changes in the position of the sputter source can have large effects on the electron beam path.

To predict the effect of the magnetic field on the electron beam trajectory, a finite element model (FEM) (COMSOL Multiphysics® version 5, AC/DC and Particle Tracing Modules) of the magnetic field produced by the magnets in a 2-in. planar magnetron sputter gun oriented in the 90° off-axis geometry was created. Additionally, the model was used to simulate the beam trajectory when passing through the magnetic field. A 2-dimensional cross-sectional view of the simulated magnetic vector field distribution can be seen in Fig. 2. The cross-section is a slice through a plane containing the heater and sputter sources, with the electron gun positioned out of the plane of the page and the phosphor screen into the plane of the page such that the electrons travel into the page. All of the working distances used for these simulations are to-scale representations of our actual chamber setup. Figure 2(a) shows the magnetic field close to the sample for the simplest case of a single gun in the off-axis geometry. Here we can note the relative field strength and additionally the direction of the field lines close to the sample. In the single gun setup the field lines point close to vertical with some tilt toward the magnets.

If we consider an electron beam traveling straight into the page at the point directly above the center of the sample in Fig. 2(a), the Lorentz force will point perpendicular to the magnetic field direction with a magnitude proportional to the field strength. Consequently, the beam will bend laterally in the x-direction towards the magnets at this point. In this way, the FEM can be used to explore more complex chamber geometries. In Fig. 2(b), a two-gun off-axis setup is shown with two sets of symmetrically facing magnets ("symmetric" setup). In the cross section, an increase in the field strength near the sample is observed (lighter blue color) along with a significantly transformed overall vector field distribution. Despite these considerable changes, the Lorentz force near the sample has similar results to that of the single gun simulation with the force pointing completely laterally in the x-direction, now with a larger magnitude.

In Fig. 2(c), the same two-gun facing geometry is shown as in Fig. 2(b) except in this case the magnet orientation of one gun is inverted such that the two guns are now in an "antisymmetric" setup. In this geometry the strength of the field near the sample is reduced (dark blue). Most notably, the magnetic field direction at the sample now points horizontally and the resulting Lorentz force near the sample points downward in the y-direction. This significant change in the magnitude and direction from both the single gun geometry and the "symmetric" setup renders the "antisymmetric" geometry more desirable from a practical point of view, as it will result in less bending.
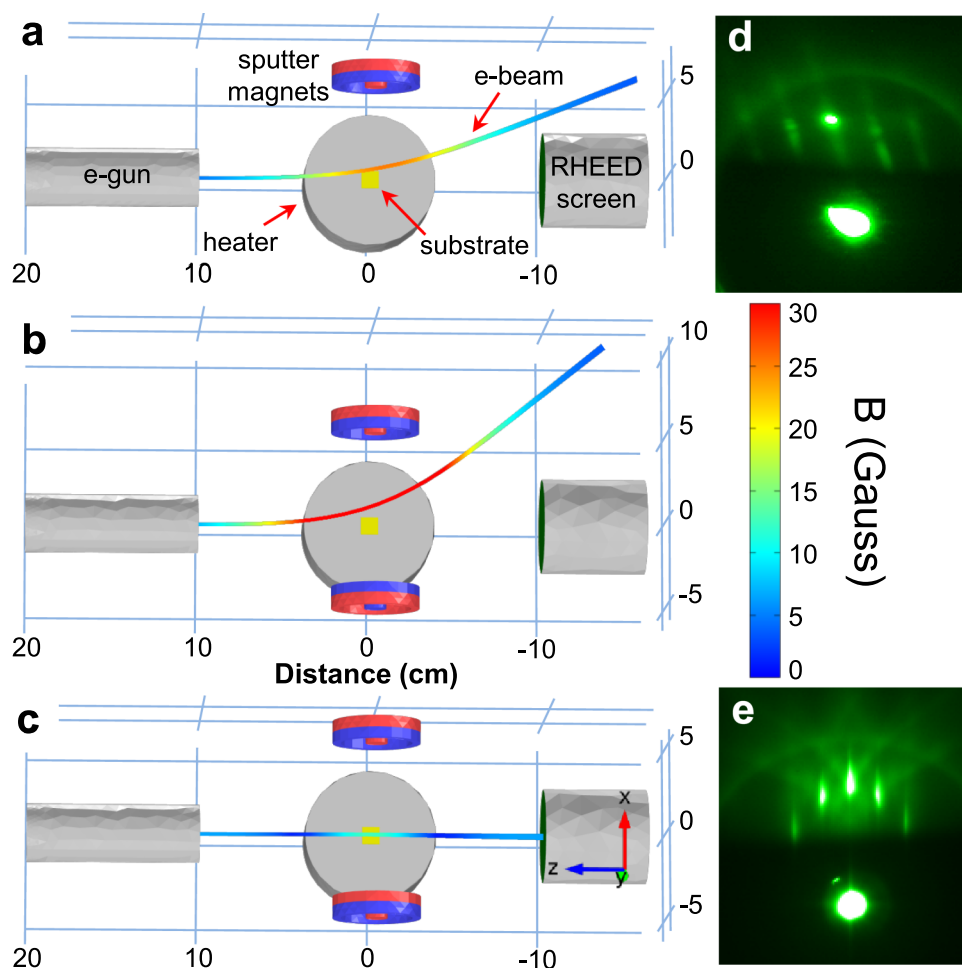
FIG. 3. *COMSOL* simulations showing electron beam deflection in single gun, symmetric, and antisymmetric sputter source geometries and their resulting RHEED pattern. (a) Single off-axis sputter source layout from a top view showing a clear deflection in the x direction is observed with the beam missing the edge of the phosphor screen. (b) Two opposite facing sputter guns in the symmetric geometry from a top view showing a more dramatic bending of the beam than in (a). (c) Antisymmetric geometry is shown resulting in moderate bending only in the y direction and striking the phosphor screen. The RHEED pattern seen in (d) is the image of a bare STO substrate in vacuum with a single sputter source in the off-axis position. Clear tilting of the pattern is observed as well as a reduction in the sharpness of the diffracted spots. (e) A RHEED image from an STO substrate is shown for the antisymmetric setup exhibiting no tilting of the pattern and sharp specular and diffracted spots.

The 2-dimensional cross sections of the magnetic field distribution shown in Fig. 2 are a good starting point for understanding the field strength and orientation near the sample surface and qualitatively predicting the electron beam deflection in different chamber geometries. However, the 2-dimensional plots make the assumption that the beam is traveling straight into the plane and do not consider the field in 3-dimensions. To quantitatively predict the electron beam path, a time-resolved finite element simulation is required, as provided by the combination of the AC/DC and particle tracing modules in FEM. Simulations can be made in the FEM that use the actual working distances in our chamber and take into account the 35 kV beam voltage used experimentally, and can also simulate hypothetical setups. This provides a useful platform for understanding what is observed and also for predicting and designing future systems. Further details related to the FEM simulations can be found in the supplementary material.

Figures 3(a)–3(c) show 3-dimensional representations and simulations of the single gun, symmetric, and antisymmetric setups, respectively. Side views of these simulations can be seen in Fig. S1 of the supplementary material. The color gradient along the beam shows the magnitude of

the magnetic field that the electrons encounter traveling from the gun to the screen. From these simulations the electron beam path can be predicted for all three cases, providing a more complete understanding of the influence of the magnetic field along the entire trajectory than the cross sectional views. Figure 3(a) shows that the deflection due to the magnetic field from a single gun is sufficient for the beam to completely miss the 55 mm diameter phosphor screen. It can be noted that the Lorentz force from the 2-dimensional cross-section (Fig. 2(a)) predicts the beam to bend not only towards the magnets but also slightly towards the heater. However, following the full trajectory in 3D the net result is that the beam is actually bent away from the heater. This is made clearer in the supplementary material Movie S1 that shows the Lorentz force on the beam as a function of time during its travel across the chamber.

Figure 3(b) shows the 3D beam trajectory in the symmetric gun setup resulting in a significantly larger deflection of the beam than observed for the single gun setup. From this, it can be concluded that using the symmetric gun setup in our chamber would make it more difficult both to have the beam diffract off the sample and have the resulting pattern strike the phosphor screen. The large lateral deflections seen in the single gun or symmetric gun geometries can be eliminated by inverting the magnetic polarity of one gun, as seen in Fig. 3(c) for the antisymmetric setup. This geometry has the additional advantage of minimizing the strength of the magnetic field along the electron beam trajectory (note the predominantly dark blue color of the beam and the field strengths indicated by the color scale), resulting in dramatically lower overall deflection of the beam. Crucially, because the field lines are parallel to the x-direction along the entire beam path, the beam is only deflected in the y-direction and can easily be made to strike the phosphor screen. Upon a careful analysis of the 3D simulations, the field lines change direction twice along the beam path leading to two zero-field points where the beam bends first up and then down then up again. This behavior is made clear in supplementary material Movie S2 that shows the Lorentz force as the beam travels across the chamber for the antisymmetric setup.

The presence of two sputter guns in the antisymmetric configuration has additional benefits beyond permitting the use of RHEED during growth. First, the growth of complex heterostructures or superlattices of two different materials would require in any case the presence of two sputter sources. Second, it has been shown that an antisymmetric sputter geometry improves film uniformity over large areas by eliminating the confined magnetic field created by a symmetric setup that leads to resputtering of deposited materials; this makes scalability more feasible.[14] These factors all point to the 2-gun antisymmetric geometry as being ideal for sputtering of complex oxides with *in situ* RHEED.

Following the logic behind the antisymmetric configuration and using the FEM, a more generic solution to the beam deflection problem can be formed. For most two gun geometries that are not purely on-axis, the antisymmetric magnets will have a similar effect to the 90° off-axis shown in Fig. 3(c). This solution is shown in greater detail in Figure S2 of the supplementary material along with a solution to the on-axis geometry where symmetric magnets are preferred.

Experimentally the results match well with what is predicted from the simulations. Without making any changes to the system, the direct beam in both the single gun and symmetric setups is not observed whereas in the antisymmetric setup the direct beam strikes the screen. However, using all of the degrees of freedom shown in Fig. 1 in our chamber, the beam can be redirected for the single gun setup such that the beam diffracts off a SrTiO$_3$ (STO) substrate and its diffraction pattern can be observed on the screen. This pattern is shown in Fig. 3(d) where the field causes the diffraction pattern to noticeably tilt, and the spots become irregularly shaped and the diffracted spots become abnormally weak. Furthermore, the Kikuchi lines typically seen on a high quality single crystal with a smooth surface are no longer observable. For the symmetric case, the deflection is so severe that the degrees of freedom are not enough to redirect the beam onto the screen and no diffraction pattern is observable. For the antisymmetric setup, very minor adjustments were required in order to observe a pattern from an STO substrate, shown in Fig. 3(e). There is no tilting present in this pattern and sharp diffraction and specular spots are observed. The pattern does show some minor streaking as a result of the magnetic field but strong Kikuchi lines are still present and the pattern is significantly more comparable to a typical STO pattern in the absence of a magnetic field.
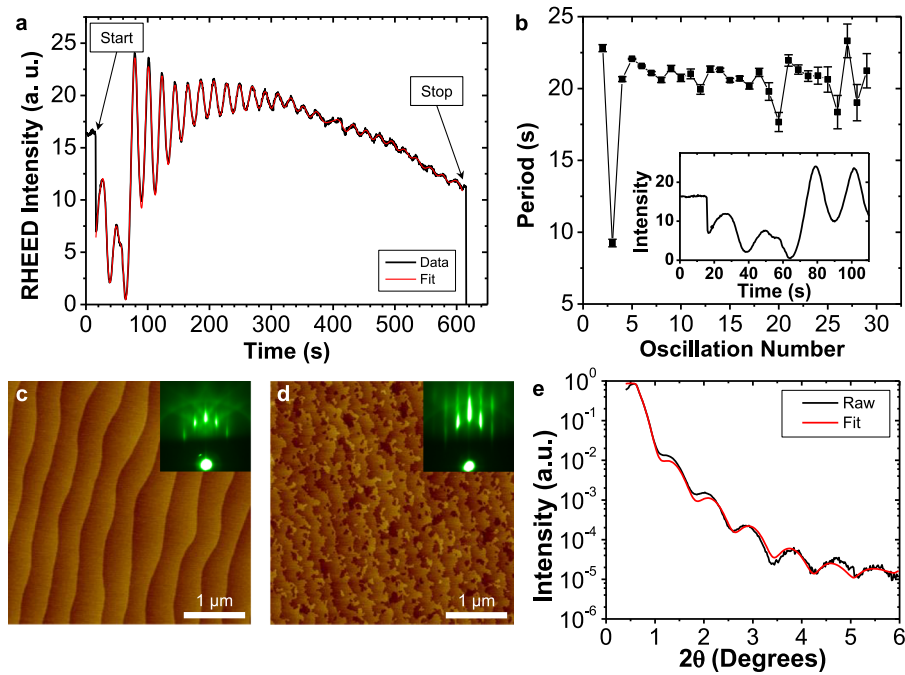
FIG. 4. RHEED intensity oscillations during SRO growth and unit cell by unit cell growth rate plot along with the corresponding AFM and RHEED images. The XRR data for the SRO film are also shown. (a) Specular spot RHEED oscillations during SRO growth on STO. The actual data are seen in black with the Gaussian fit in red. Clear oscillations are observed corresponding to one unit cell of growth. (b) The peak to peak period for each unit cell of growth is shown. The inset highlights the first few oscillations where the extended period can be seen due to the termination conversion during SRO growth. (c) AFM image of the STO substrate prior to growth showing smooth step and terrace structure. The inset shows the RHEED image of the STO substrate in vacuum before growth. (d) AFM image of the SRO surface showing single unit cell steps and incomplete step edges. The inset shows the RHEED image of the SRO film with sharp spots after the growth in vacuum and no tilting of the pattern. (e) The XRR data (black line) and fits (red line) provide an accurate thickness estimation of 10.9 nm, and indicate the high quality of the surface and interface.

This confirms the simulation results that the antisymmetric configuration is the ideal setup for *in situ* sputtering with RHEED for 90° off-axis growth.

As previously mentioned, high partial pressures of argon (Ar) gas necessary for creating the sputtering plasma are an additional concern when considering real time analysis of RHEED. While background gas pressures can be similar for sputtering and high-pressure PLD[15] (~0.2 Torr), Ar has a scattering cross-section for electrons that is ~4 times larger than oxygen[16] resulting in reduced diffracted intensities and a higher diffuse background that reduces the total dynamic range that can be measured. This effect is further demonstrated in Figure S3 of the supplementary material. The scattering can be mitigated by increasing the energy of the electrons and by decreasing the distance between the aperture of the beam source and the phosphor screen. Our beam energy is 35 keV (the upper limit of the electron gun) and our working distance is 18 cm, although shorter distances are recommended. It should be noted that higher energies lead to a larger Ewald's sphere, and both the larger Ewald's sphere and the shorter working distance lead to a contraction of the RHEED pattern spacing and subsequently a decrease in the lateral resolution of the diffracted spots. Thus, further optimization of the beam energy and working distance must be done for each individual chamber design.

Using the magnetic field modeling and the high-pressure considerations discussed above, we have grown SRO thin films on STO substrates in the antisymmetric 90° off-axis geometry with *in situ* RHEED. Oscillations of the RHEED specular spot (SS) intensity during the deposition are readily observable, as shown in Fig. 4(a) (diffracted spot intensity is shown in Fig. S4 of the supplementary material), and permit the calibration of the deposition of single unit cells and allow the identification of layer-by-layer growth mode, as discussed below. To our knowledge, these are

the first RHEED oscillations demonstrated for any sputter growth. A Gaussian fit of the oscillations (the red line in Fig. 4(a)) was used to obtain the crest-to-crest period of each oscillation, and a plot of these periods is shown in Fig. 4(b). After the initial few unit cells, the growth rate is fairly constant throughout with an average period of 20.7 s.

The STO substrates are treated to form a TiO_2 termination[17] prior to growth, and the corresponding atomic force microscopy (AFM) image exhibits a single unit-cell step-and-terrace structure with nearly straight step edges as shown in Fig. 4(c). The inset to Fig. 4(c) shows the RHEED image of the STO substrate prior to growth in vacuum; the sharp diffracted and specular spots confirm the high quality crystalline substrate and smooth surface. The inset in Fig. 4(d) shows the RHEED images taken in vacuum after the SRO growth. The diffraction pattern still shows sharp spots with some minimal streaking suggesting a high degree of crystallinity in the film and a predominantly two-dimensional surface. Further crystallinity confirmation by x-ray diffraction can be seen in Figure S5 in the supplementary material. The AFM image in Fig. 4(d) shows a clear step-and-terrace structure with single unit-cell step height and shows some small single unit cell islands on the terraces. This morphology is comparable to SRO films grown on STO by PLD,[18] but the existence of the small islands on the sputter grown film may be an indication of nucleation sites corresponding to the layer-by-layer growth deduced from the extended RHEED specular spot oscillations. The AFM result also confirms observations from the RHEED pattern that the film surface is atomically smooth.

The film thickness determined by the x-ray reflectivity (XRR) scan confirms that each RHEED oscillation corresponds to the deposition of a single unit cell as shown in Fig. 4(e). The fit suggests that the surface and interface are smooth and the density is uniform throughout, and yields a total film thickness of 10.9 nm corresponding to a growth rate of 21.7 s per unit cell. This rate agrees well with the 20.7 s per unit cell steady state rate acquired from the RHEED oscillations in Fig. 4(b). This confirmation has several implications. First, observation of RHEED oscillations allows for an *in situ*, real time capability to control sputter deposition at the level of a single unit cell. Second, extended RHEED oscillations identify a layer-by-layer growth mode for SRO by sputtering, unlike step-flow growth mode that characterizes SRO deposition by PLD after the first few unit cells.[19] Third, analysis of the RHEED oscillations at the start of growth allows the identification of a surface termination inversion in the first few unit cells of deposition. As shown more clearly in the inset of Fig. 4(b) as the shoulder to the second peak, the period from the first peak to the shoulder is 1.5 times the steady-state period. The termination inversion from RuO_2 to SrO in the first few unit cells reported here for sputtering is similar to that reported for SRO growth by PLD.[18] However, in contrast to PLD growth, the SRO does not transition from layer-by-layer to step flow growth after the termination inversion. The extended RHEED oscillations that characterize layer-by-layer growth by sputtering allow real time calibration and control of film thickness to the unit-cell level, as compared to the time or pulse based calibration required for the step-flow growth mode by PLD.

In conclusion, combining sputter deposition with *in situ* RHEED is an inherently challenging task due to the strong magnetic fields and high pressures that adversely affect the electron beam. Unlike PLD and MBE which have standardized growth geometries, sputtering covers a wide range of arrangements from on-axis to 90° off-axis. Thus, finite element modeling of the magnetic fields and electron beam trajectories for the specific sputtering chamber geometry is advised but we have demonstrated a simple solution which can be used for many layouts. In this work we have developed a simple geometry to curtail the bending in an off-axis geometry configuration by having two sputter guns facing one another with antisymmetric magnet polarities. As a consequence, we have been able to observe the first specular spot intensity oscillations associated with layer-by-layer growth during sputter growth. The existence of extended specular spot oscillations during $SrRuO_3$ deposition, not seen in PLD growth, creates a new avenue for research including precise super-lattices that contain SRO as a layer. We have also observed extended specular spot oscillations during the sputter growth of LSMO and LAO films, as shown in Figure S6 of the supplementary material, suggesting that the RHEED technique is useful during the sputter growth of many different materials. In all cases, using RHEED as an *in situ* monitoring technique during deposition improves the reproducibility of sputter grown films by providing real time digital control over the thickness, giving real time feedback on film quality and roughness throughout the growth, leading to faster

optimization of thin film processes. RHEED plays a critical role in the deposition of epitaxial thin films in both molecular beam epitaxy as well as pulsed laser deposition already and should become equally as fundamental in sputter deposition. Since sputtering is such a common technique due to its industrial and scientific relevance, and relatively low cost we believe that this work will make RHEED a more readily available *in situ* tool for sputter growth. Our approach applies to many different geometries and can be used for the growth of a wide range of thin film materials including metals, oxides, nitrides, and carbides, where precise unit cell control is essential.

See the supplementary material for further description of the experiments and more detailed finite element model analysis.

[1] C. E. C. Wood and B. A. Joyce, J. Appl. Phys. **49**(9), 4854 (1978).

[2] J. J. Harris, B. A. Joyce, and P. J. Dobson, Surf. Sci. **103**(1), L90 (1981).

[3] W. Braun, *Applied RHEED: Reflection High-Energy Electron Diffraction During Crystal Growth* (Springer Science & Business Media, 1999).

[4] I. Bozovic and J. N. Eckstein, MRS Bull. **20**(5), 32 (1995).

[5] G. J. H. M. Rijnders, G. Koster, D. H. A. Blank, and H. Rogalla, Appl. Phys. Lett. **70**(14), 1888 (1997).

[6] J. A. Venables, G. D. T. Spiller, and M. Hanbucken, Rep. Prog. Phys. **47**(4), 399 (1984).

[7] J. A. Venables, *Introduction to Surface and Thin Film Processes* (Cambridge University Press, 2000).

[8] C. B. Eom, R. J. Cava, R. M. Fleming, J. M. Phillips, R. B. Vandover, J. H. Marshall, J. W. Hsu, J. J. Krajewski, and W. F. Peck, Jr., Science **258**(5089), 1766 (1992).

[9] T. Tybell, C. H. Ahn, and J. M. Triscone, Appl. Phys. Lett. **75**(6), 856 (1999).

[10] A. Lin, X. Hong, V. Wood, A. A. Verevkin, C. H. Ahn, R. A. McKee, F. J. Walker, and E. D. Specht, Appl. Phys. Lett. **78**(14), 2034 (2001).

[11] M. Gibert, P. Zubko, R. Scherwitzl, J. Iniguez, and J. M. Triscone, Nat. Mater. **11**(3), 195 (2012).

[12] B. Peters, A. Alfonsov, C. G. F. Blum, S. J. Hageman, P. M. Woodward, S. Wurmehl, B. Buchner, and F. Y. Yang, Appl. Phys. Lett. **103**(16), 162404 (2013).

[13] E. B. Svedberg, J. Birch, C. N. L. Edvardsson, and J. E. Sundgren, Surf. Sci. **431**(1-3), 16 (1999).

[14] N. Newman, B. F. Cole, S. M. Garrison, K. Char, and R. C. Taber, IEEE Trans. Magn. **27**(2), 1276 (1991).

[15] C. B. Eom, J. Z. Sun, B. M. Lairson, S. K. Streiffer, A. F. Marshall, K. Yamamoto, S. M. Anlage, J. C. Bravman, T. H. Geballe, S. S. Laderman, R. C. Taber, and R. D. Jacowitz, Physica C **171**(3-4), 354 (1990).

[16] A. Jablonski, F. Salvat, and C. J. Powell, *NIST Electron Elastic-Scattering Cross-Section Database* (National Institute of Standards and Technology, Gaithersburg, MD, 2010).

[17] M. Kawasaki, K. Takahashi, T. Maeda, R. Tsuchiya, M. Shinohara, O. Ishiyama, T. Yonezawa, M. Yoshimoto, and H. Koinuma, Science **266**(5190), 1540 (1994).

[18] G. Rijnders, D. H. A. Blank, J. Choi, and C. B. Eom, Appl. Phys. Lett. **84**(4), 505 (2004).

[19] J. Choi, C. B. Eom, G. Rijnders, H. Rogalla, and D. H. A. Blank, Appl. Phys. Lett. **79**(10), 1447 (2001).